

# Supporting Information For: Cross Photoreaction of Glyoxylic and Pyruvic Acids in Model Aqueous Aerosol

---

*Sha-Sha Xia, Alexis J. Eugene, and Marcelo I. Guzman \**

Department of Chemistry, University of Kentucky, Lexington, Kentucky 40506, United States

\*Corresponding author's email: marcelo.guzman@uky.edu

---

## The Journal of Physical Chemistry A

---

<b>Content</b>	<b>Page</b>
Additional Environmental Considerations	S2
Calculation of [GA] <sub>0</sub> and [PA] <sub>0</sub> in a Mixture via UV-visible Spectroscopy	S3
Additional Experimental Methods for NMR Analysis	S4
Alternative Reaction Mechanisms Considered	S9
Table S1. Controls with PA	S5
Figure S1. <sup>13</sup> C NMR Spectra for the Region of Ether Groups	S5
Figure S2. Normalized Area under UV-visible Absorption Spectra for PA Photolysis	S6
Figure S3. Areas under ESI-MS Peaks with <i>m/z</i> 127 and 129	S6
Figure S4. Structures of the Two Diastereomers of 2,3-Dimethyltartaric Acid	S7
Figure S5. <sup>1</sup> H NMR spectra for Experiment with a Mixture of GA and PA	S7
Figure S6. HSQC Analysis for 6 h Photolysis of a Mixture of GA and PA	S7
Figure S7. gCOSY Before and After 6 h Photolysis of the Mixture of GA and PA	S8
Figure S8. UHPLC-MS for Hydrazones of the Experiment with GA and PA	S9
Scheme S1. Considered Mechanism for the Cross Reaction of Aqueous GA and PA	S10
Scheme S2. Considered Mechanism for the Cross Reaction of Aqueous GA and PA	S11
Scheme S3. Considered Mechanism for the Cross Reaction of Aqueous GA and PA	S12
Scheme S4. Considered Mechanism for the Cross Reaction of Aqueous GA and PA	S13
Scheme S5. Considered Mechanism for the Cross Reaction of Aqueous GA and PA	S14
Scheme S6. Considered Mechanism for the Cross Reaction of Aqueous GA and PA	S15
References	S16

## Additional Environmental Considerations

All samples for photolysis studies are prepared after assuming that the upper limit to the water content of aerosol droplets is determined by the deliquescence curve of an ammonium bisulfate solution<sup>1,2</sup> at 50 % relative humidity (RH). For such conditions, the droplets in aerosols contain 0.6 g of H<sub>2</sub>O/g of SO<sub>4</sub><sup>2-</sup> or a pyruvic acid concentration [PA] > 20 mM under very acidic conditions.<sup>3</sup> Similarly, the concentration of glyoxylic acid, [GA], in arctic secondary organic aerosol (SOA) can be estimated,<sup>4</sup> to be as high as 287 mM, for a molar ratio [GA]/[PA] ~ 8-14. Even higher concentration can be used in laboratory experiments that simulate a polluted environment, because the level of PA and GA in a city such as Tokyo can exceed by 30 and 3 times, respectively, those measured in the pristine Arctic aerosol.<sup>4,5</sup>

Additionally, experimental conditions of ionic strengths, temperature, and photon flux are chosen to simulate those encountered by nascent sea spray aerosols mixing with pollution at coastal regions. The model starting mixtures contain *ca.* [PA] = 28.0 mM and [GA] = 236.0 mM, which are exposed to UV-visible light in the range of surface solar radiation. The variables under study include samples with and without the most abundant electrolytes in seawater ([Na<sup>+</sup>] = 468 mM, [Cl<sup>-</sup>] = 545 mM and [SO<sub>4</sub><sup>2-</sup>] = 28.2 mM)<sup>6</sup> under a 1 atm N<sub>2</sub>(g), 1 atm O<sub>2</sub>(g), and 1 atm air. This work presents an advanced analysis that contrasts how the chemical composition and optical properties of model aqueous SOAs vary during photochemical and thermal processes.

### Calculation of Initial [GA] and [PA] in a Mixture via UV-visible Absorption Spectroscopy

Actual initial concentrations of PA and GA in the mixture are determined by UV-visible absorption spectroscopy analysis using Beer's Law (Equation S1)

$$A = \varepsilon b[X] \tag{S1}$$

where  $\varepsilon$  is the molar absorption coefficient,  $b$  is the optical path length, and  $[X]$  is the concentration of the component. Considering that the absorption bands of pure GA and pure PA significantly overlap in their mixture, a method to resolve their concentrations is introduced using a least square analysis. For this purpose, the individual spectra of standard  $[PA] = 28.8$  mM and  $[GA] = 90.3$  mM is recorded. The absorbance at wavelength  $\lambda = 260, 270, 280, 290, 300,$  and  $320$  nm from each one of the standards, and their mixture ( $A_m$ , the same sample in Figure 1) is extracted. Then, the molar absorption coefficient of both PA and GA can be solved for each wavelength using Beer's Law. Spectral data is imported to a spreadsheet in Microsoft Excel for the previous purpose, where Equation S2

$$A = \varepsilon(X) b [X] + \varepsilon(Y) b [Y] \tag{S2}$$

is employed to calculate the absorbance ( $A_{cal}$ ) for the mixture of GA and PA at each wavelength from the estimated concentrations  $[GA]_{guess}$  and  $[PA]_{guess}$  (two estimated values). Then, using the Microsoft Excel Solver function, the least square conditions, which minimize the sum of squares of  $(A_{cal} - A_m)^2$  by iteratively varying the guess values  $[GA]_{guess}$  and  $[PA]_{guess}$ , the solution to the concentrations in the mixture is provided. The actual initial concentrations in the mixture of a typical experiment are  $[GA] = 235.6$  mM and  $[PA] = 27.9$  mM.<sup>7</sup>

### **Additional Experimental Methods for NMR Analysis**

For  $^1\text{H}$  NMR spectroscopy, data was collected at 298 K, with 32 K complex points, using a  $90^\circ$  pulse length (measured for each sample,  $\sim 14.5 \mu\text{s}$ ). Thirty-two scans were acquired with a spectral width of 6.419 kHz, an acquisition time of 1.276 s, and a relaxation delay of 1.0 s. The water suppression enhanced through T1 effects (WET) method applied to all proton spectra was set up from the software VnmrJ 3.2 with a bandwidth of 100 MHz. The  $^1\text{H}$  NMR spectra for the same experiment with a mixture of GA and PA displayed in Figure 6 is presented in this Supporting Information document. The  $^1\text{H}$  NMR peaks in the spectra provide information of the hydrogen atoms located in different positions, particularly at  $\delta = 8.25$ , 5.38, 2.46 and 1.58 ppm, correspond to GA, the gem-diol form of GA, the methyl groups of PA, and the methyl groups of the gem-diol form of PA, respectively. DSS at  $\delta = 0.00$  ppm is used as a reference.

The HSQC spectrum reporting the correlation of protons and carbons via single-bond correlation<sup>7</sup> for the experiment with a mixture of GA and PA (as in Figure 6) is also provided in this document.

For  $^{13}\text{C}$  NMR spectroscopy, data was collected at 298 K, with 64 K complex points, using a  $90^\circ$  pulse length (measured for each sample,  $\sim 9.1 \mu\text{s}$ ). About 24000 scans were acquired with a spectral width of 25.1731 kHz, an acquisition time of 1.302 s, and a relaxation delay of 1.0 s.

For 2D gCOSY and HSQC 2D NMR experiments, the methods were built from the default experiments in VnmrJ 3.2 with the same conditions for proton and carbon spectra described above. The same WET method was also applied to proton spectra in 2D NMR, which provides the chemical shift information from  $^1\text{H}$  and  $^{13}\text{C}$  NMR. 2D NMR also offers the through-bond correlation between couples of protons on adjacent carbons in gCOSY measurements, and the correlation between proton and carbon via single-bond in HSQC experiments.<sup>7</sup> The same gCOSY method is applied to DSS internal standard (that also serves as a reference with  $\delta = 0.00$  ppm), GA, PA, and the mixture of GA and PA under the conditions of the experiment before and after photolysis. The gCOSY spectra is color coded for DSS (grey), GA (green), PA (red), and the mixture of GA and PA (blue). From both combined spectra, no signals could be observed for the correlation of two adjacent carbon atoms both having hydrogen atoms except the ones from DSS. The only coupled proton correlations registered are from the methylene groups in DSS ( $\delta = 0.62$ , 1.77, and 2.92 ppm). Thus, the likelihood of observing  $>\text{CH}-\text{CH}<$  groups in the product mixture is low. The signal intensity for the mixture of products at the cross point of 8.33 ppm, which corresponds to the range of aldehyde hydrogens, is considerably larger than the spectrum before photolysis, pointing to the existence of photoproducts with aldehyde groups.

**Table S1.** Controls with PA.

	Conditions				
	$h\nu$	Electrolytes	Atmosphere		
			Air	N <sub>2</sub>	O <sub>2</sub>
Control G	✓	✓	✓		
Control H	✓	✓		✓	
Control I	✓	✓			✓
Control J	✓		✓		
Control K	✓			✓	
Control L	✓				✓
Control M		✓	✓		

Key:  $h\nu$  indicates the presence of light. Conditions: pH 1.0 and the electrolytes were  $[\text{Na}^+] = 545 \text{ mM}$ ,  $[\text{SO}_4^{2-}] = 28.2 \text{ mM}$ , and  $[\text{Cl}^-] = 468 \text{ mM}$ .

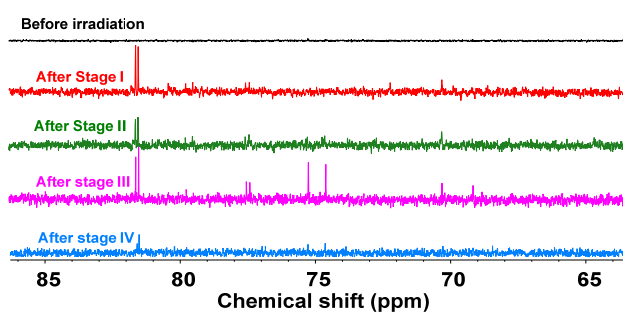


**Figure S1.** <sup>13</sup>C NMR spectra for the region of ether groups in the experiment of Figure 1 (black) before irradiation and after (red) stage I, (green) stage II, (pink) stage III and (blue) stage IV in Scheme 2.

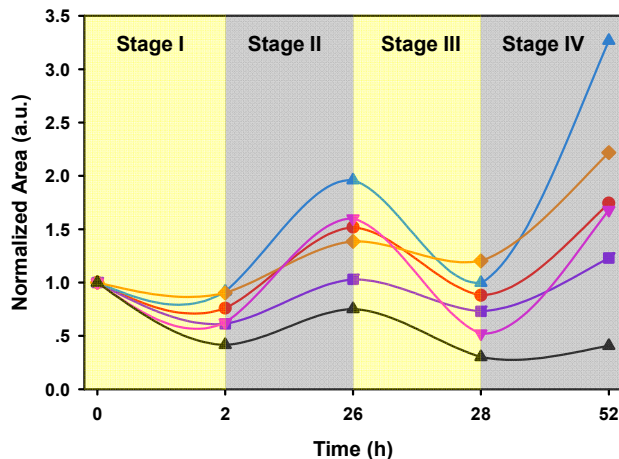


**Figure S2.** Normalized area under UV-visible absorption spectra ( $\lambda_{\min} = 295$  nm and  $\lambda_{\max} = 500$  nm) for controls of PA photolysis in Table S1 for the four stages in Scheme 1. Key: (red ●) control G for the photolysis of 26.0 mM PA with electrolytes in air at pH 1.0. (Blue ▲) control H in  $N_2$ , (pink ▼) control I in  $O_2$ , (violet ■) control J without electrolytes, (orange ◆) control K without electrolytes in  $N_2$ , and (black ▲) control L without electrolytes in  $O_2$ . Control M in the absence of light remained stable over the four stages and is not included.

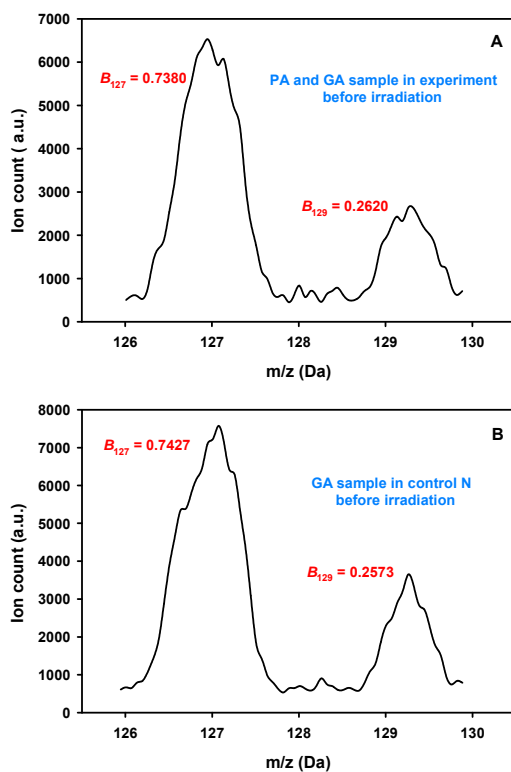


**Figure S3.** Areas under ESI-MS peaks with  $m/z$  127 and 129 for samples before irradiation for (A) a mixture of GA and PA in the experiment of Figure 1 and (B) a GA solution with electrolytes in air at pH 1.0.

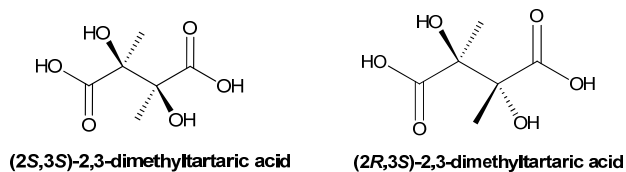


**Figure S4.** Structures of the two diastereomers of 2,3-dimethyltartaric acid ( $m/z$  177).

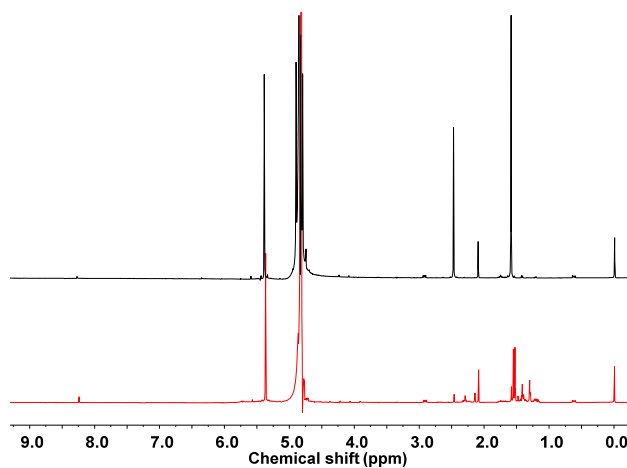


**Figure S5.**  $^1\text{H}$  NMR spectra for the experiment with a mixture of GA and PA (as in Figure 6) before (top black trace) and after 6 h photolysis (bottom red trace).

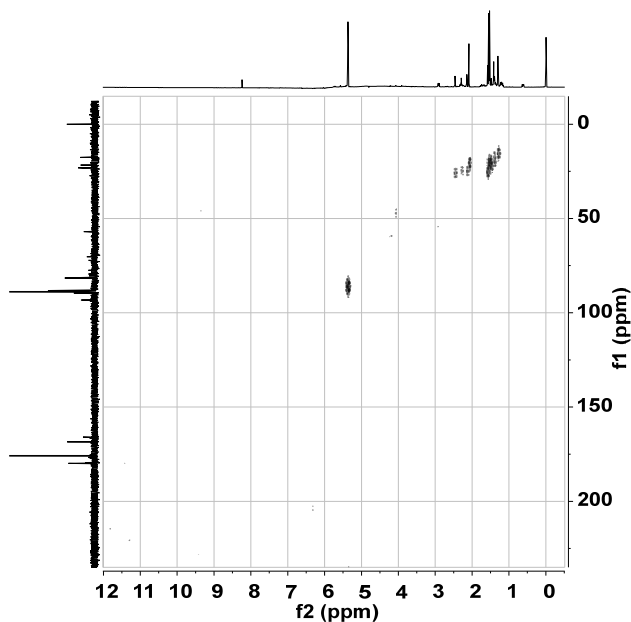


**Figure S6.** HSQC solvent (water) peak subtracted spectra of a mixture of 235.6 mM GA and 27.9 mM PA with electrolytes in air (experiment in Table 1) after 6 h photolysis (Stage I in Scheme 2).

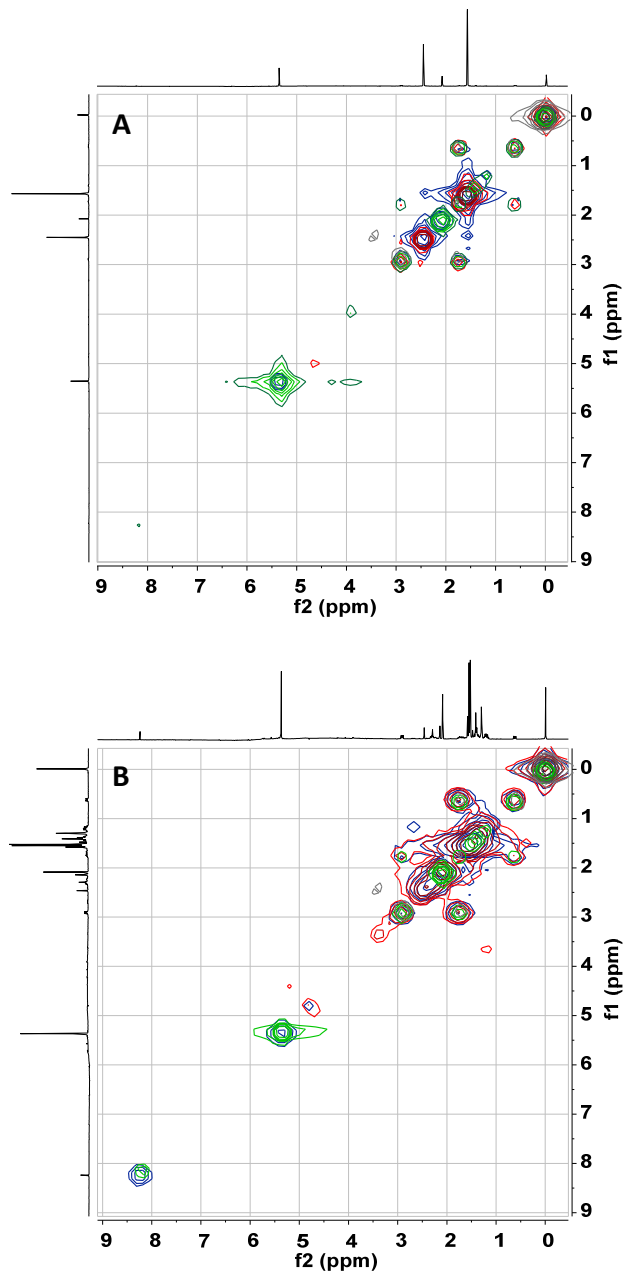


**Figure S7.** gCOSY registered using WET suppression and water peak subtraction for (green) 235.6 mM GA and (red) 27.9 mM PA (blue) mixed solution for the experiment in Table 1 with (grey) DSS internal standard(A) before and (B) after 6 h photolysis.

## UHPLC- MS Analysis of Hydrazones

For carbonyl analysis, 26  $\mu\text{L}$  of the sample was diluted to 5 mL with water. To this solution, 5 mL of 25 mM 2,4-dinitrophenylhydrazine (DNPH, Sigma, HPLC grade, 99.6%) in acetonitrile (EMD Millipore, LC-MS grade, 99.99%) with 4% (v/v) sulfuric acid (Acros, 95.6%) was added. In the negative ionization mode DNPH adds a mass of 180 Da to the hydrazone of the originating monoanion. The mixture was inverted for mixing and allowed to incubate at room temperature for 1 h. After incubation, 750  $\mu\text{L}$  of the derivatized mixture was diluted 1:1 with acetonitrile. This final dilution was analyzed by UHPLC-MS.

After derivatization, 25  $\mu\text{L}$  of the samples containing the hydrazones were injected and separated on a Thermo Scientific Accela 1250 UHPLC equipped with a photodiode array detector set at 360 nm and an ESI-MS (negative mode) detector (MSQ Plus). The separation used a reversed phase C18 column (Agilent, Zorbax Eclipse Plus C18 RRHD,  $2.1 \times 100$  mm,  $1.8 \mu\text{m}$ ) using a solvent gradient of (A) 5 mM formic acid (Fisher Optima LC-MS grade) and (B) 5 mM formic acid in acetonitrile at a flow rate of  $400 \mu\text{L min}^{-1}$ . The initial conditions were 17% B for 5 min, which was then ramped to 60% over 9 min. Ionization conditions were set to cover the  $m/z$  range 40-740 and utilized a drying gas temperature of  $400 \text{ }^\circ\text{C}$ , a nebulizer voltage of  $-2.4 \text{ kV}$ , a cone voltage of  $-25 \text{ V}$ , and a nebulizer pressure of 70 psi  $\text{N}_2(\text{g})$ .

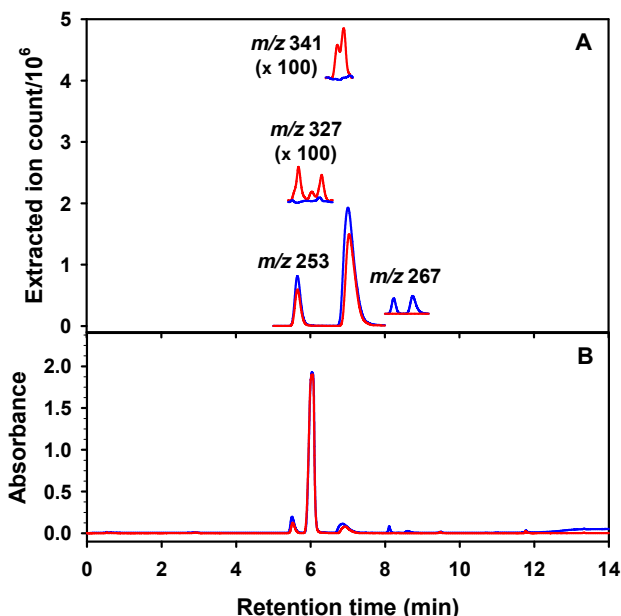
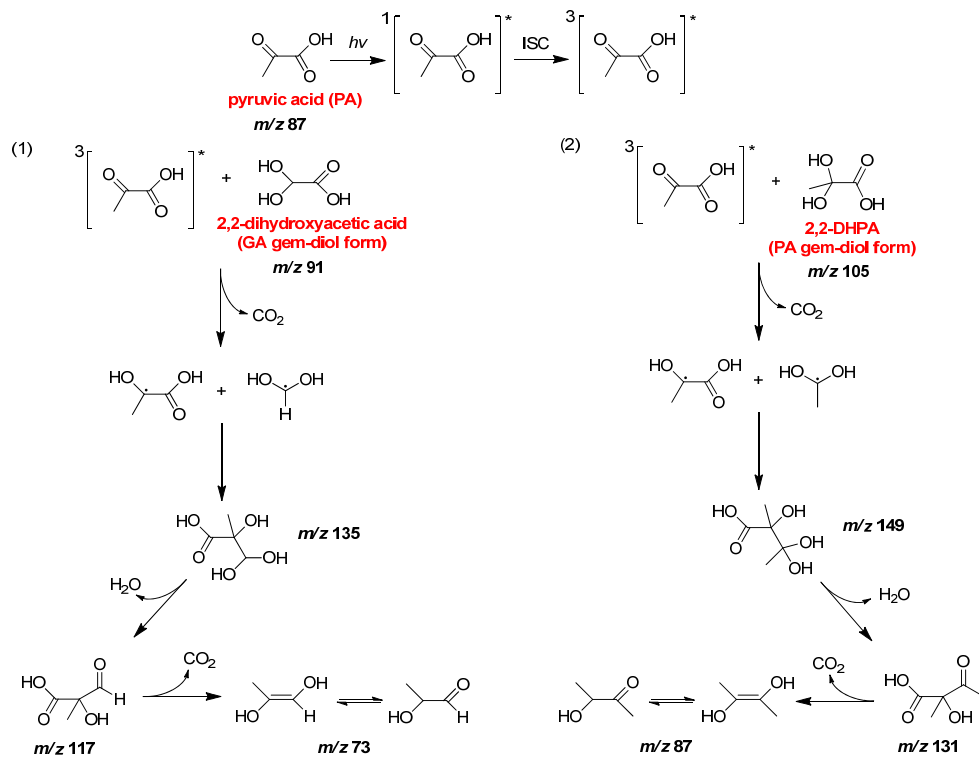


**Figure S8.** UHPLC with (A) MS and (B) UV detection at 360 nm for hydrazones (blue) before and (red) after 6 h photolysis for the experiment in Figure 1 of the paper. The only hydrazones observed at  $m/z$  253 and 267 decrease over time and correspond to those of GA (MW 74) and PA (MW 88), respectively. The new peaks at  $m/z$  327 and 341 correspond to the cross-products with MW 148 and 162, respectively. No peaks are detected for the cross-product with MW 164 at  $m/z$  343.

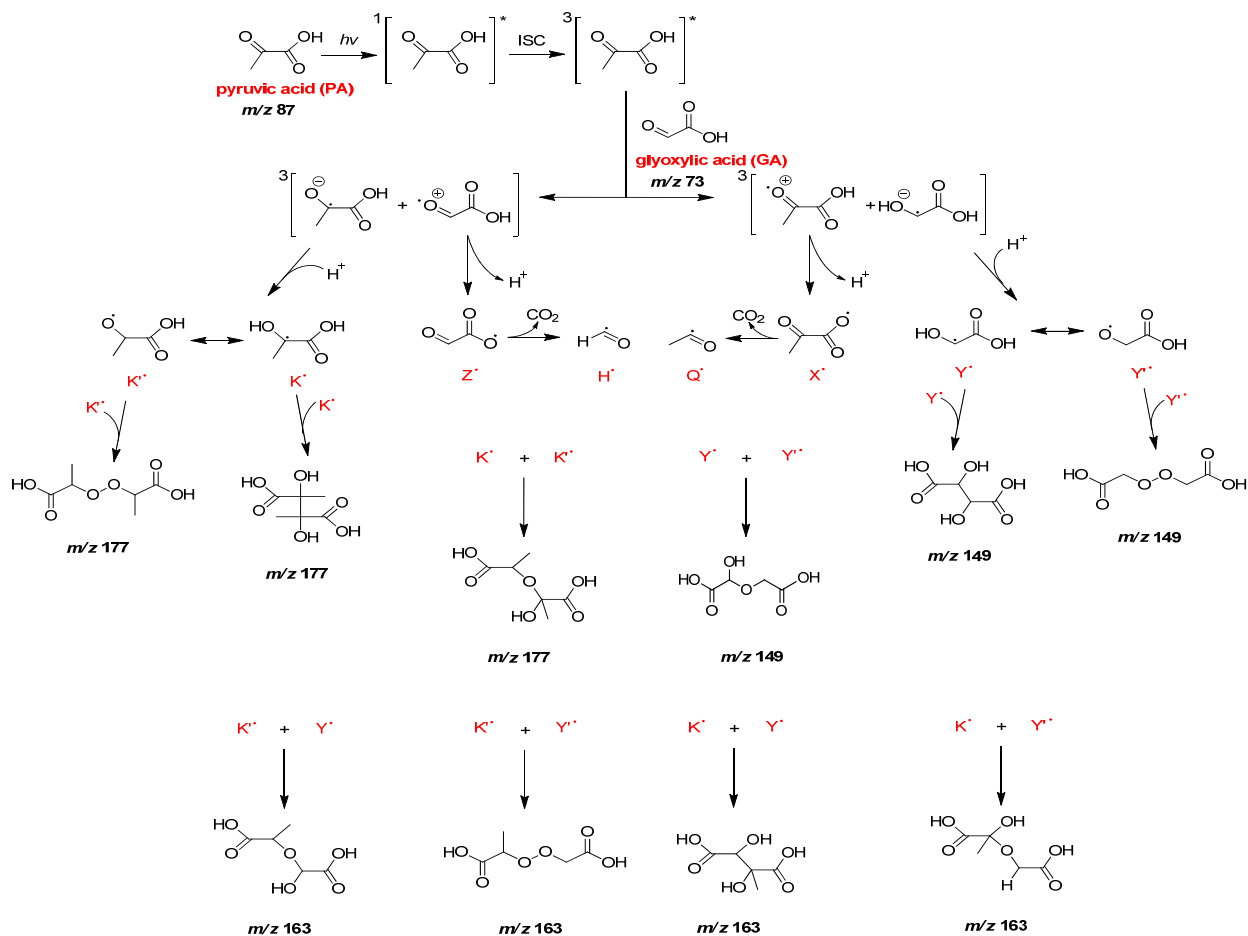
## Alternative Reaction Mechanisms Considered

Scheme S1 considers the possible H-abstraction from the gem-diol of PA from preformed radicals, in the mechanism of cross reaction of GA and PA. If this pathway would be of importance, the mechanism in Scheme S1 would predict the formation of intermediates and products with formula mass 136, 118, 150, 132, 88, and 74 Da. However, the final products acetoin (88 Da) and 2-hydroxypropanaldehyde (74 Da) possess a carbonyl that should have reacted with DNPH to be detected after chromatographic separation by UHPLC-ESI-MS.<sup>8</sup> In addition, the underivatized sample did not display the anions at  $m/z = 135$ , 117 and 131 in the IC-MS chromatogram. Therefore, it can be concluded that the mechanism in Scheme S1 is not competing with the proposed mechanism in Scheme 2.

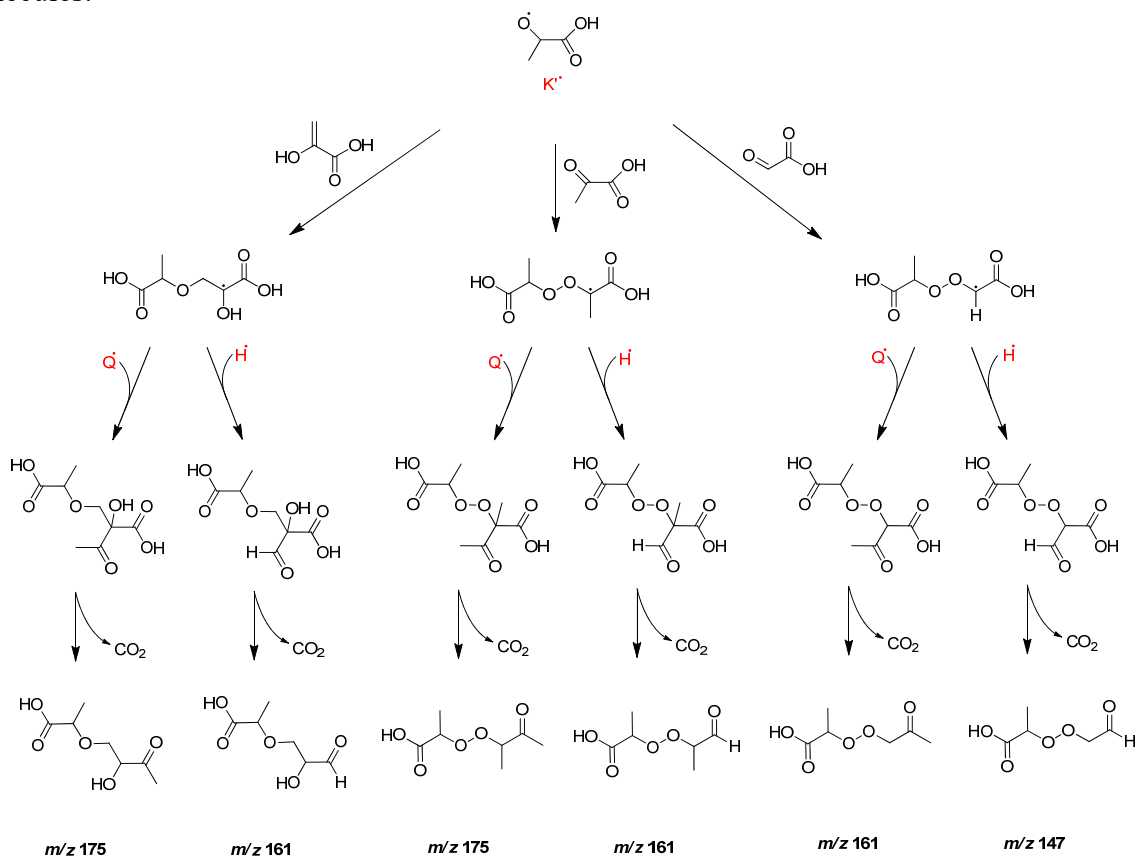
**Scheme S1.** Considered Mechanism for the Cross Reaction of Aqueous GA and PA with Hydrogen Abstraction from the Gem-diol of PA.



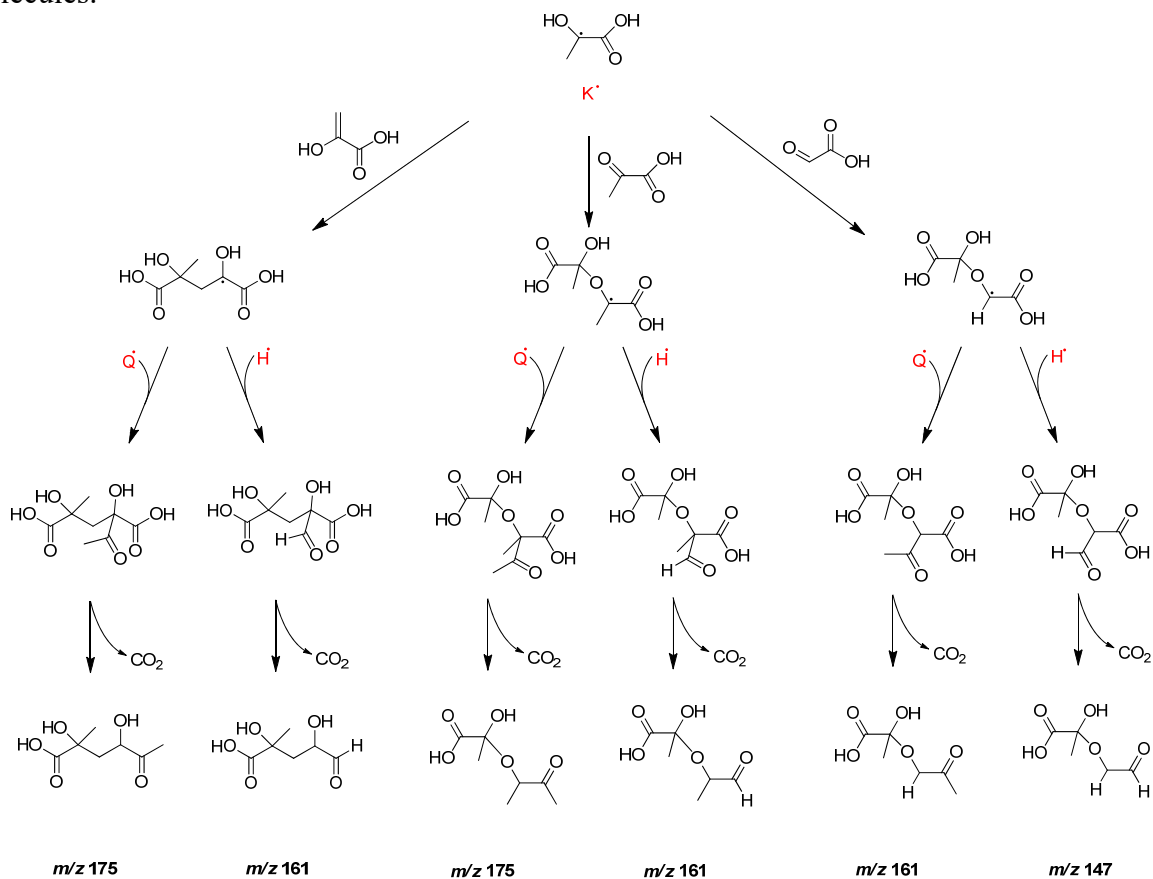
**Scheme S2.** Considered Mechanism for the Cross Reaction of Aqueous GA and PA with Alternative Pathways to those Presented in Scheme 2.



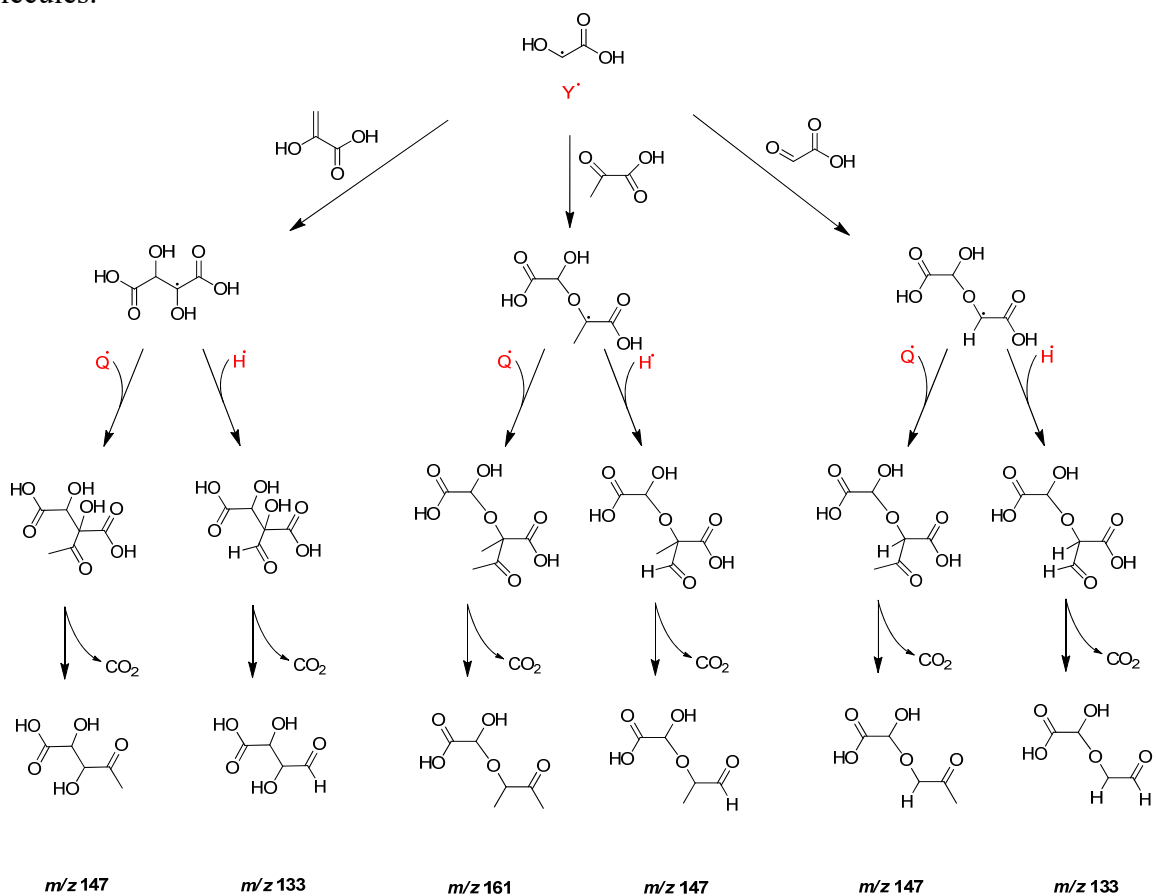
**Scheme S3.** Considered Reactions of Oxyl radical  $K^{\bullet}$  from PA in Scheme S2 with Neutral Molecules.



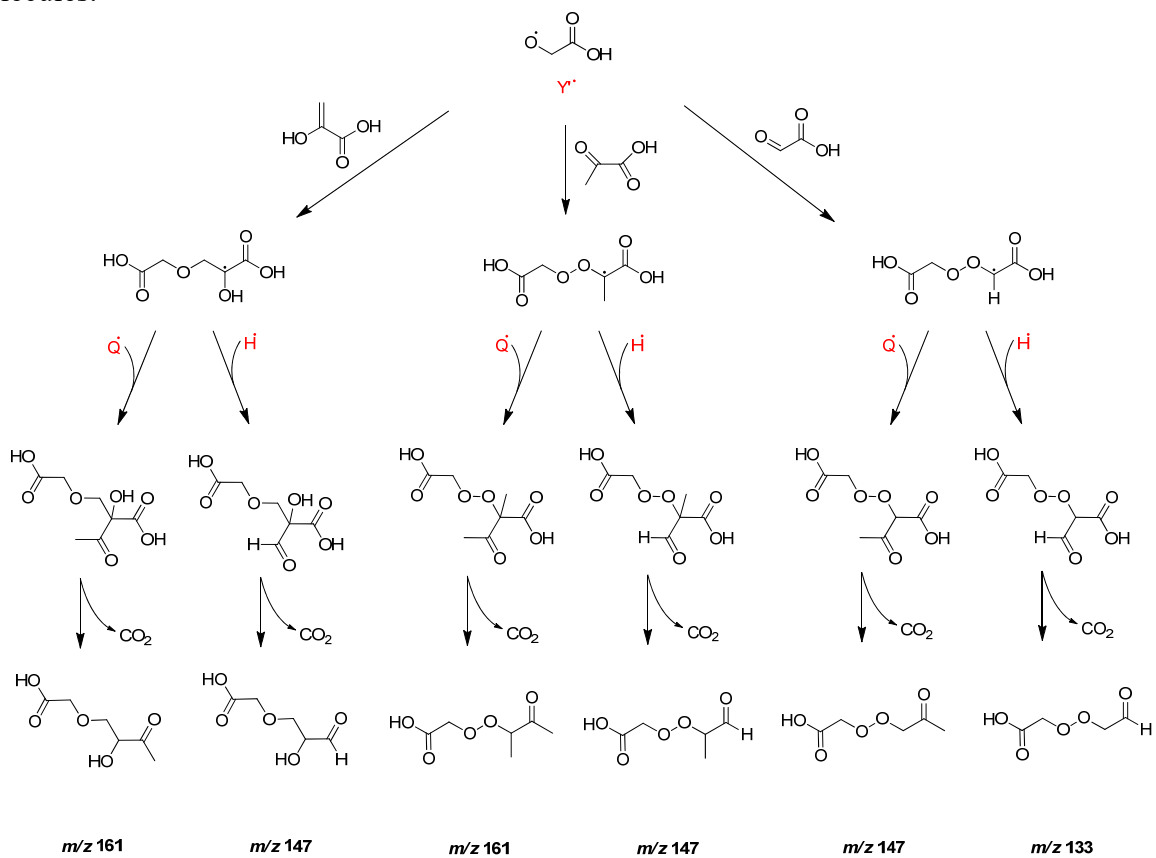
**Scheme S4.** Considered Reactions of Ketyl Radical  $K^{\bullet}$  from PA in Scheme S2 with Neutral Molecules.



**Scheme S5.** Considered Reactions of Ketyl Radical  $Y^{\bullet}$  from GA in Scheme S2 with Neutral Molecules.



**Scheme S6.** Considered Reactions of Oxyl Radical Y<sup>•</sup> from GA in Scheme S2 with Neutral Molecules.



## References

- (1) Saxena, P.; Hildemann, L. M. Water absorption by organics: Survey of laboratory evidence and evaluation of UNIFAC for estimating water activity. *Environ. Sci. Technol.* **1997**, *31*, 3318-3324.
- (2) Jang, M.; Czoschke, N. M.; Northcross, A. L. Atmospheric Organic Aerosol Production by Heterogeneous Acid-Catalyzed Reactions. *ChemPhysChem* **2004**, *5*, 1646-1661.
- (3) Guzman, M. I.; Colussi, A. J.; Hoffmann, M. R. Photoinduced oligomerization of aqueous pyruvic acid. *J. Phys. Chem. A* **2006**, *110*, 3619-3626.
- (4) Kawamura, K.; Imai, Y.; Barrie, L. A. Photochemical production and loss of organic acids in high Arctic aerosols during long-range transport and polar sunrise ozone depletion events. *Atmos. Environ.* **2005**, *39*, 599-614.
- (5) Kawamura, K.; Yasui, O. Diurnal changes in the distribution of dicarboxylic acids, ketocarboxylic acids and dicarbonyls in the urban Tokyo atmosphere. *Atmos. Environ.* **2005**, *39*, 1945-1960.
- (6) Harvey, H. W. *The chemistry and fertility of sea waters*, 2<sup>nd</sup> ed.; Cambridge University Press: New York, NY, 1957.
- (7) Pavia, D.; Lampman, G.; Kriz, G. *Introduction to spectroscopy*, 3<sup>rd</sup> ed.; Brooks/Cole USA, 2003.
- (8) Eugene, A. J.; Guzman, M. I. Reactivity of ketyl and acetyl radicals from direct solar actinic photolysis of aqueous pyruvic acid. *J. Phys. Chem. A* **2017**, *121*, 2924-2935.